Available online at www.sciencedirect.com

SCIENCE DIRECT®

Thin Solid Films 478 (2005) 338–344

thin solid films

www.elsevier.com/locate/tsf

Interface detection in poly-ethylene terephthalate–metal laminates using variable energy positron annihilation

R. Escobar Galindo[a], H. Schut[a], A. van Veen[a], R. Rastogi[b], W.P. Vellinga[b,*], H.E.H. Meijer[b]

[a]*Defects in Materials, Interfaculty Reactor Institute, Delft University of Technology, 2629JB Delft, The Netherlands*
[b]*Materials Technology, Mechanical Engineering, Eindhoven University of Technology, P.O. Box 513, Whoog 4.145, 3524 CK, 5600 MB Eindhoven, The Netherlands*

Received 19 February 2004; accepted in revised form 1 November 2004
Available online 9 December 2004

Abstract

Thin coatings of poly-ethylene terephthalate (PET) on metal ("laminates") have been studied with a variable energy positron annihilation technique. A correlation between PET crystallinity and the positron annihilation parameter *S* related to the free volume in the polymer is found. It is shown that buried interfaces in these systems may be detected provided the *S* parameter of the polymer coating is lower than that of the substrate and higher than that of the surface. Also it is found that large positron diffusion lengths in the substrate favour interface detection. Further, changes in *S* parameter of PET–metal laminates were measured during uniaxial deformation and shown to be in qualitative accordance with a very simple model description that accounts for changes in free volume in PET during plastic deformation as well as the area fraction of cracks occurring in the PET.

Keywords: Interfaces; Positron spectroscopy; Polymers; Adhesion

1. Introduction

In modern engineering, composites of polymers and metals appear ever more frequently. Many examples occur in the micro-electronic industry, but there are also applications as structural materials in automotive and shipping industry, or as protective coatings in food packaging. In such laminates, the mechanical properties of the base materials as well as the interfacial adhesion between them are important in determining the forming limits and lifetime during their intended use.

The starting point of the present study are poly-ethylene terephthalate (PET)–metal laminates employed in food-packaging industry. PET is a popular coating material for food-packaging and has been approved by the Food and Drug Agency. In coatings, PET may appear in semicrystalline form for which the microstructure (e.g. crystallinity and lamellar width) and the resulting mechanical behavior depend sensitively on the thermomechanical history. A number of papers has been devoted to resolving structure-property relations of this type of PET, e.g. Refs. [1,2]. Alternatively glycol-modified forms may be used that remain amorphous regardless of the thermomechanical treatment. The mechanical behavior of the PET–steel laminates has been the subject of recent work [3,4] where the focus was on the relative mechanical stability of coatings with widely differing microstructure during uniaxial strain.

In contrast, in this paper, the main point of interest are microstructural changes occurring near the interface of such laminates during forming processes.

Positron annihilation techniques offer a non-destructive means of obtaining microstructural parameters (in particular of porosity, or "free volume", on a (sub)nanometer scale) that are relevant for the mechanical behavior of polymers and metals. Moreover, recently, these capabilities have been applied to the study of buried interfaces [5]. One of the aims

* Corresponding author. Tel.: +31 40 247 2920; fax: +31 40 247 7355.
E-mail address: w.p.vellinga@tue.nl (W.P. Vellinga).

0040-6090/$ - see front matter © 2004 Elsevier B.V. All rights reserved.
doi:10.1016/j.tsf.2004.11.045

of the work presented in this paper was therefore to explore the possibilities of applying positron annihilation techniques to the study of polymer–metal laminates and especially polymer–metal interfaces.

In glassy polymers, the fraction of free volume, the average pore size and size distribution associated with it are known to influence relaxation spectra, mobility of segments and various transport phenomena [6,7]. For example, according to Mininni et al. [6], the modes of molecular motion that contribute to ductility and toughness are sensitive to the free volume fraction.

When a positron is implanted from a vacuum into a polymer film the positron survives before annihilation either as an unbounded positron, or in the form of a positronium "atom" (Ps) by picking up an electron from the polymer molecules. Positronium can exist in two forms, depending on the spins of the electron and positron. In *para*-positronium (*p*-Ps), the spins are anti-parallel and, in *ortho*-positronium (*o*-Ps), they are parallel. In solids, annihilation of *p*-Ps and *o*-Ps may involve a two-process. The component of the momentum of the electron–positron pair parallel to the direction of emission of the photons leads to an energy shift of the order of a few keV (with respect to the annihilation energy per photon of 511 keV). The resulting Doppler Broadening of the peak at 511 keV may be measured, a technique that is known as Doppler Broadening of Annihilation Radiation (DBAR). It is common practice to introduce two dimensionless parameters, *S* and *W*, to define the shape of the Doppler Broadened peak. The *S* parameter is defined as the ratio between the area of the central part of the annihilation peak and the total area of the peak and indicates the fraction of positrons that annihilate with low momentum electrons (valence or conduction electrons). The *W* parameter is defined in an analogous fashion using the tails of the distribution and indicates annihilation events with high-energy (core) electrons.

Since the density of high-energy electrons near defects is reduced, annihilation is more likely to involve valence electrons, leading to an increase in the *S* parameter.

The sensitivity of positrons to open volumes makes them useful for the study of atomic-scale defects and nanometer-scale porosity and positron annihilation spectroscopy has been used extensively in determining microstructural properties of defects in many materials [5] and the technique has been applied in the study of polymers and polymeric coatings. The technique has been demonstrated of being capable of determining size, size distribution and anisotropic structure of pores and free volume in polymers [8]. In fact, changes in the physical properties of polymers on exposure to various weathering agents showed excellent correlation with a number of positron annihilation parameters [8,9].

Positron beam annihilation techniques are well suited to detect defect evolution caused by mechanical deformation. However, few such studies have been carried out in-situ [10,11]. Increasing the incident energy of positrons, open volumes may be studied at ever increasing depths beneath a surface, including those near buried interfaces and, in fact, the technique has been shown to provide a non-destructive method to study interfaces [5,12].

In the DBAR experiments reported here, *S* and *W* parameters are measured as a function of positron implantation energy or depth below the coating surface, using a variable energy positron beam (VEP, see below). Moreover, experiments were performed on samples deformed ex-situ in uniaxial tension.

In this paper, two issues are addressed. Firstly, the detection of buried interfaces in polymer–metal laminates with DBAR and, secondly, changes in the accessible physical parameters caused by uniaxial tensile deformation of PET–metal laminates. Moreover, this is studied for differing PET microstructures, amorphous and semicrystalline.

2. Experimental

The polymers used were PET and PETG, which is a glycol-modified non-crystallizing PET. The PET used has a Mw 52,000 kg/mol and a Mn 26,000 kg/mol. The Mw of PETG is not known, but since the above mentioned PET was used for the synthesis of PETG through an extra processing step, Mw of PETG is assumed to be lower than of PET.

2.1. Sample preparation

PET coatings were prepared by spin-coating PET dissolved in 1,1,1,3,3,3,hexauoro 2-isopropanol on the following substrates: interstitial free steel (IF), electrochemically chromium-coated steel (ECCS), Al and Si wafer. The metal substrate were rolled sheets and as a consequence showed a rough surface. The IF steel and some of the Al substrates were polished mechanically with diamond suspensions down to 1 μm and subsequently given a mirror-like finish with colloidal silica suspensions. The IF substrates were annealed at 1000 K for 1 h in vacuum of typically 10^{-5} Pa. Spin-coating resulted in semicrystalline PET coatings (sc:PET) after evaporation of the solvent. To obtain amorphous PET coatings (a:PET), samples were briefly heated to T_m, and then quenched to room temperature. Semicrystalline PET coatings were subsequently obtained in two different ways: by glass-crystallization (Gl:PET–metal) or melt-crystallization (Me:PET–metal). Gl:PET–metal laminates were heated from room temperature, kept at (170 or 210 °C) for 10 min and were subsequently quenched; Me:PET–metal laminates were slowly cooled from T_m to room temperature. Crystallinity of the films was estimated with Fourier transform infrared spectroscopy [4]. The crystallinity of the Gl:PET coatings ,Gl170 43%, Gl210 45%, was lower than that of the Me:PET coatings, 56%. The final thickness, *d*, of the coatings was between 0.3 and 4 μm. Characteristics of all samples studied are summarized in Table 1. Substrate dimensions were 10×50 mm^2. Laminates were uniaxially deformed in tension in a Deben Microtest tensile stage at a

Table 1
Summary of samples studied

Substrate	PET	d (μm)	Interface detection
ECCS	a	1.5	no
	Gl	2.3	no
IF steel	a	1.2	no
Al polished	a	1.5	yes
Al unpolished	Gl	3.2	no
	Me	4	no
Si	a	1.5	yes
ECCS	PETG	2	no
IF steel	PETG	2	no
	PETG	0.3	no

speed of 0.2 mm/min. Deformation was performed in-situ in a reaction polarization optical microscope.

2.2. DBAR data analysis

Positron beam analysis was performed using the Delft Variable Energy Positron beam [13]. The positrons are injected into the samples with energies tuned between 100 eV and 25 keV, at room temperature in a vacuum of about 10^{-6} Pa. The maximum implantation energy corresponds to a typical mean implantation depth of 2 μm in materials with a density of 3 g cm^{-3}. In the present study, DBAR is applied using a variable energy positron beam. The data is analyzed with the aid of the VEPFIT [14] and SWAN [15] codes. VEPFIT provides an algorithm that simulates the implantation of positrons and solves the diffusion equation, taking into account the trapping and annihilation of the positrons in a layered material. Measured values of $S(E)$ and $W(E)$ are a sum of the characteristic S_i and W_i values of the trapping layers i weighted by the fraction of positrons trapped in each layer $f_i(E)$, given by:

$$S(E) = \sum_{i=1}^{N} f_i(E) S_i \quad (1)$$

$$W(E) = \sum_{i=1}^{N} f_i(E) W_i \quad (2)$$

where

$$\sum_{i=1}^{N} f_i(E) = 1 \quad (3)$$

and N is the number of trapping layers.

In Fig. 1, characteristic S and W values for some reference materials are shown. Both parameters can be combined in "S–W maps" with a third variable (i.e. implantation energy, depth, annealing temperature or strain) as running parameter. In such S–W maps, physically different positron annihilation sites show up as clustered points and may be characterized.

Such plots may be very helpful in exposing detail that may not be obvious from S vs. E plots and only available after detailed fitting. (Application of S–W maps to the well-known SiO_2/SiO system can be found in Refs. [16,17]).

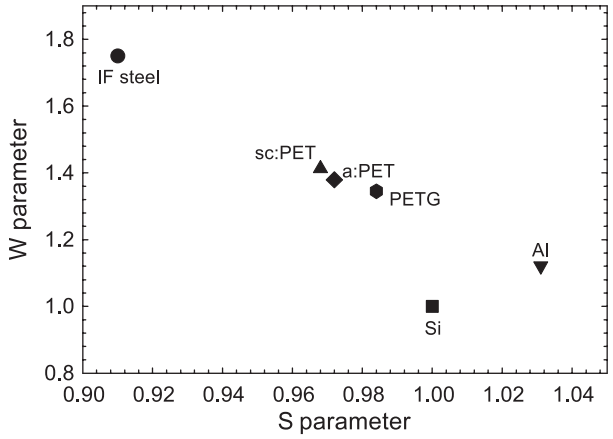

Fig. 1. S–W map with reference values of relevant materials, normalized with respect to values of single crystalline Si.

The SWAN program allows for determination of such S–W cluster points, the characterization of annihilation sites and calculation of the annihilation fractions of positrons at the sites.

S and W values presented have been normalized with respect to the S and W values of single crystalline Si, 0.585 and 0.027, respectively, unless indicated otherwise.

3. Results and discussion of DBAR experiments

3.1. S for various types of PET

Fig. 2 shows the value of the S parameter of the PET coatings vs. density of the coatings. The density of PETG is 1.2 g/cm^3, that of amorphous PET is approximately 1.33 g/cm^3 and that of (hypothetical) pure crystalline PET is 1.44 g/cm^3. Densities of semicrystalline PET were estimated from the crystallinity measurements mentioned earlier. For increasing crystallinity, a decrease in S value is observed,

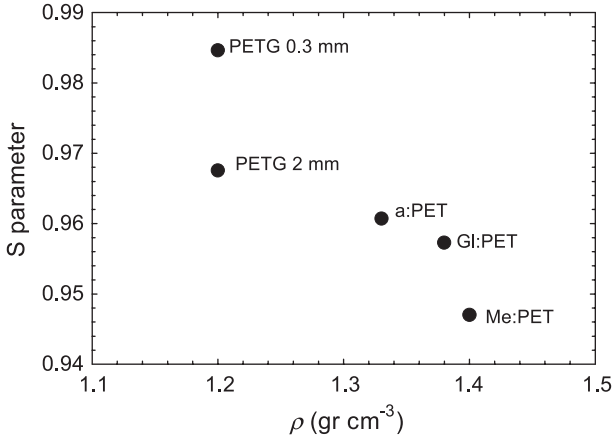

Fig. 2. Normalized S (see text) vs. density of PET coatings.

which indicates that the free volume decreases with increasing crystallinity and increasing density. Interestingly, the *S* parameter of the very thin spin-coated PETG film (0.3 μm) is much higher than that of the 2-μm spin-coated PETG coating, indicating a higher free volume.

3.2. Interface identification

Two examples of the DBAR experiments for PET coatings on steel are illustrated in Fig. 3, which shows measurements on PETG–IF and a:PET–ECCS laminates.

The results in Fig. 3 show clear evidence of only three annihilation sites, indicated as 1, 2 and 3 in Fig. 3(b). The coating surface (1) is seen to have a lower *S* value than the coating (2) due to the formation of Ps in the bulk of the polymer.

The *S* parameter increases toward the bulk of the coatings and subsequently shows a plateau representing the bulk PET *S* value (2). Finally, *S* shows a gradual decrease towards a lower value expected for a steel substrate (3). From the *S*–*W* maps in Fig. 3(b), it is clear that the *S*–*W* pairs are on straight lines from the surface (1) to the coating (2) and from the coating (2) to the substrate (3) positions.

Remarkably, to fit the results, it is not necessary to include an annihilation site specific to the interface.

However, an annihilation site specific to the interface is anticipated as the structure of the interface should be different from that of either bulk PET or bulk metal and the apparent absence of such a site requires explanation.

The absence of a site specific to the interface in these particular experimental results may be explained firstly by hypothesizing that the interface structure is relatively open compared to either metal or PET and secondly by a short diffusion length of positron in the substrates. If the PET–metal interface is open then, in fact, the positrons annihilate not in a close interface but in the internal surfaces of the PET and the metal. Therefore, the *S* value of the interface would be a combination of the *S* values of both surfaces. As those values are both lower than the polymer bulk and also the metal has a lower *S* value than the polymer bulk, the interfacial *S* is masked in an *S* vs. *E* curve. Similar behaviour occurs for *W* but in this case the polymer bulk has a higher value than the polymer and metal surfaces and also higher than the metal bulk. Hence, in an *S*–*W* map, the experimental points lay in a straight line from the cluster point of the polymer bulk to the metal without showing the presence of the interface. In Ref. [18], Holgado et al. also showed the masking of the interface between zirconia coatings and silicon substrates. In that case, the *S* value of the coating bulk was lower than the coating surface and the substrate bulk. That is opposite to the case of our coatings but with similar observations (no need of an interface in the fitting).

Furthermore, efficient detection of the interface depends on the capability of positrons implanted in the substrate to diffuse back to the interface. In case of a short diffusion length, the fraction of positrons annihilating at the interface is roughly speaking equal to the fraction directly implanted at that interface. In this case, the SW point associated with the interface only shows up in an SW plot when the *S* or *W* value differs substantially from those of the substrate and polymer layer. In addition, in absence of this difference fitting of the *S* (or *W*) vs. positron implantation energy (*E*) curves can be achieved without introducing an interface layer. In case positrons can diffuse from the bulk to the interface, fitting of *S* (or *W*) vs. *E* requires an interface causing trapping the diffusing positrons. Although the steel samples we used as substrates were mechanically polished and annealed, some defects might still be present.

These are taken to be the main reasons for the fact that the DBAR experiments performed on the PET–steel samples did not show a clear indication of the polymer–metal interface.

In order to overcome these problems posed by the identification of PET–steel interfaces with positron annihilation, interfaces of PET with other substrates were studied. Good candidates should have a higher *S*, a lower *W* and a longer diffusion length than steel. From Fig. 1, it can be concluded that both Si and Al fulfill the *S*–*W* conditions.

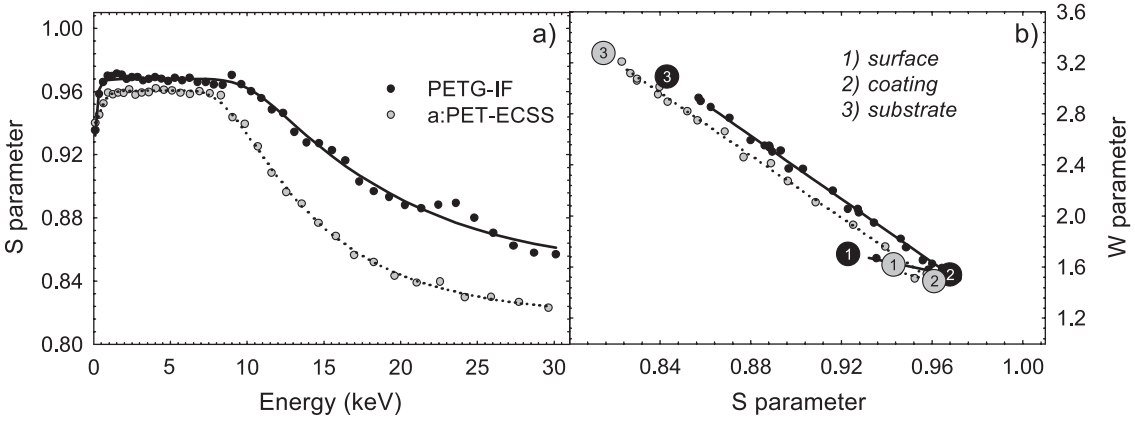

Fig. 3. (a) Normalized *S* as a function of positron implantation energy for a:PET–ECCS and PETG–IF laminates. (b) *S*–*W* maps for the same coatings. The positron annihilation sites are assigned to: (1) surface, (2) coating and (3) substrate. Solid lines represent VEPFIT fits.

Positron diffusion lengths in Si and polished Al were estimated to be of 200 and 100 nm, respectively. Hence, PET was deposited on these substrates.

Indeed, in similar measurements of a:PET coatings on single crystal Si and polished Al substrates, the interfaces are clearly observed. In Fig. 4a, it can be seen that, for a:PET–Si and a:PET–Al laminates, the *S* parameter first reaches the value of the coating (0.96). Then, with increasing implantation energy, *S* decreases indicating the presence of the interface before increasing again towards the substrate *S* value. The *S*–*W* maps shown in Fig. 4b make this observation much clearer. The interface (simulated as a 5-nm-thick perfect positron trap (diffusion length=1 nm)) is now characterized by a separate *S*–*W* cluster point (3) very close to the Al surface value of 1.5. This is indeed consistent with the existence of a more open structure at the interface.

It is noteworthy that for a PET–Al in which the interfaces was rather rough as the Al was not polished prior to coating, the PET–Al interface could not be detected, either from the *S* vs. *E* graphs, or from fitting *S*–*W* maps in the way discussed above.

3.3. Laminates in uniaxial tension

On uniaxial tensile loading of the laminates, the deformation mode of the PET depends on its initial microstructure. Amorphous PET coatings show massive shear-banding of the coating as well as "cracks" (that are actually tiny localised necks) that are restricted to the coatings, i.e. they do not expose the underlying metal substrate. Semicrystalline PET coatings fail predominantly by cracking, and cracks do reach the substrate [3,4].

The positron results may be related to these types of behaviour. Fig. 5 shows the PET bulk *S*-parameter as a function of strain. For clarity, in this figure the *S* parameter values have been normalized to their values at zero strain. Small increases in *S* are observed for the laminates of amorphous PET and are thought to be related to changes in structure of the amorphous PET on straining. A comparatively high increase of *S* is observed in the Me:PET–Al laminate and a comparatively large decrease is observed for the Gl:PET–IF laminate. As this correlates with the *S* values of the substrates, the changes observed in *S* are likely due to an increase of positron annihilation in the respective

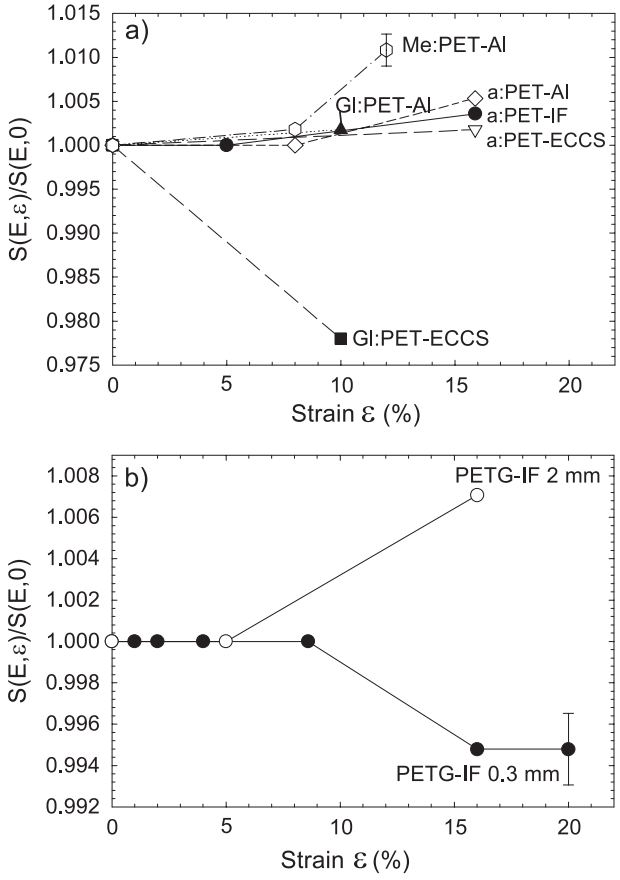

Fig. 5. Normalized *S* vs. strain for PET (top) and PETG (bottom) coatings, deposited on different metal substrates. Values of *S* used for normalisation are the values for the bulk of the respective coatings as obtained from VEPFIT analysis. For samples with a gradient in *S* and *W*, the average of the minimum and maximum value is plotted here.

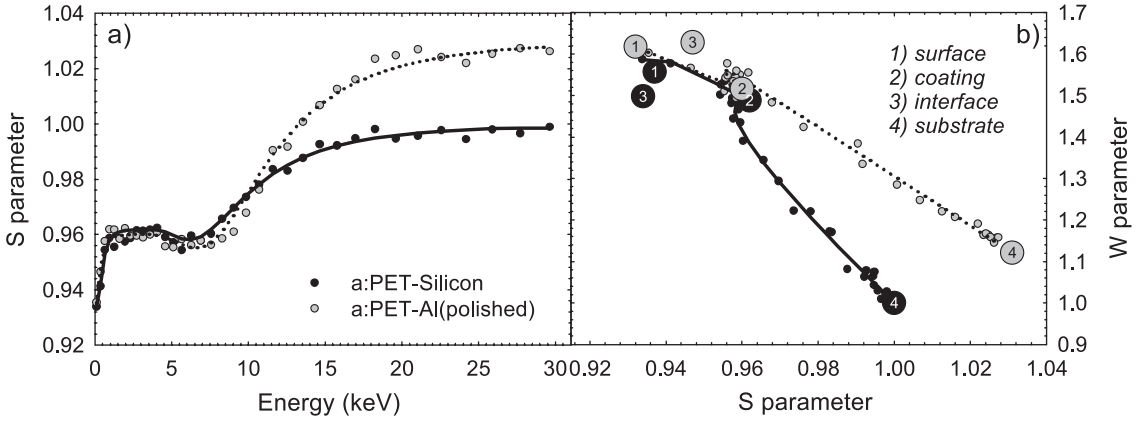

Fig. 4. (a) normalized *S* vs. average implantation energy of PETG–IF and a:PET–ECCS laminates. (b) *S*–*W* maps for these coatings showing four positron annihilation sites: (1) surface, (2) a:PET, (3) interface and (4) substrate. Solid lines represent VEPFIT analysis results.

Table 2
Normalized S and W before and after uniaxial tensile deformation, and deformation mode of PET

Substrate	PET	d (μm)	Strain (%)	S	W	Open cracks
ECCS	a	1.5	0	0.961	1.481	–
			16	0.962	1.481	–
	Gl	2.3	0	0.957	1.519	–
			10	0.943–0.929	1.589–1.786	+
IF	a	1.2	0	0.954	1.630	–
			16	0.957	1.519	–
Al, polished	a	1.5	0	0.961	1.519	–
			15	0.966	1.418	–
Al, unpolished	Gl	3.2	0	0.957	1.519	–
			10	0.959	1.418	+
	Me	4	0	0.947	1.519	–
			12	0.952–0.962	1.499–1.356	+
IF	PETG	2	0	0.968	1.555	–
			16	0.974	1.407	–
IF	PETG	0.3	0, 1, 2, 4, 9	0.985	1.295	–
			16, 20	0.979	1.350	–

Where two values are mentioned a gradient of the parameter as a function of depth existed and values shown represent the minimum and maximum measured.

substrates due to the appearance of cracks in the coatings, which can be observed with optical microscopy.

So, straining the laminate is expected to change the S parameter of the PET layers in two different ways. Firstly, there may be an effect on the S value of the PET layers because the probed free volume may change as a function of strain, for example in the case that shear bands and localised necks appear. Secondly, if cracks appear, that cover a certain area fraction $f_s(\varepsilon)$, the measured value of S will be influenced since part of the positrons now annihilate in the substrate.Consequently, $S(E,\varepsilon)$ is expected to behave as:

$$S(E,\varepsilon) = f_s(\varepsilon)S_s(E,\varepsilon) + (1 - f_s(\varepsilon))S_{\mathrm{PET}}(E,\varepsilon). \quad (4)$$

If no cracks occur, an increasing strain ε is expected to lead to higher values of $S(E,\varepsilon)$ because of an increased defect density of the coating (effect 1). If cracks do occur, the S parameter of the substrate is also probed, which is expected to lead to a decrease in $S(E,\varepsilon)$ if $S_s(E,\varepsilon)<S_{\mathrm{PET}}(E,\varepsilon)$ and an increase if $S_s(E,\varepsilon)>S_{\mathrm{PET}}(E,\varepsilon)$. This would be the case for all energies E (effect 2).

So, considering the deformation behavior of the PET–steel laminates, one would expect the laminates with amorphous PET coatings to show effect 1 only, and the laminates with semicrystalline PET to show both effects 1 and 2.

For the laminates with amorphous PET coating where cracks do not reach the substrate, a small increase in $S(E,\varepsilon)$ (at energies E related to the PET coating) is expected due to the increased defects density in the coating. Indeed, this is found in the uniaxially strained samples, as SPET increases from 0.961 to 0.966 for a:PET–Al laminates, from 0.954 to 0.957 for a:PET IF and from 0.968 to 0.974 for the PETG–IF. The increase from 0.961 to 0.962 for a:PET–ECCS is not considered to be significant. The increase in $S(E,\varepsilon)$ is smaller than or of the same order as the differences encountered between the different types of PET as shown in Fig. 2.

For the laminates with sc:PET, one would expect potentially a much larger effect, of the order of $f_s(\varepsilon)(S_{\mathrm{PET}}-S_s)$, considering the substantial differences in S_{PET}, S_{Al} and S_{IF}. VEP-DBAR results are shown in Table 2 and in Figs. 5 and 6.

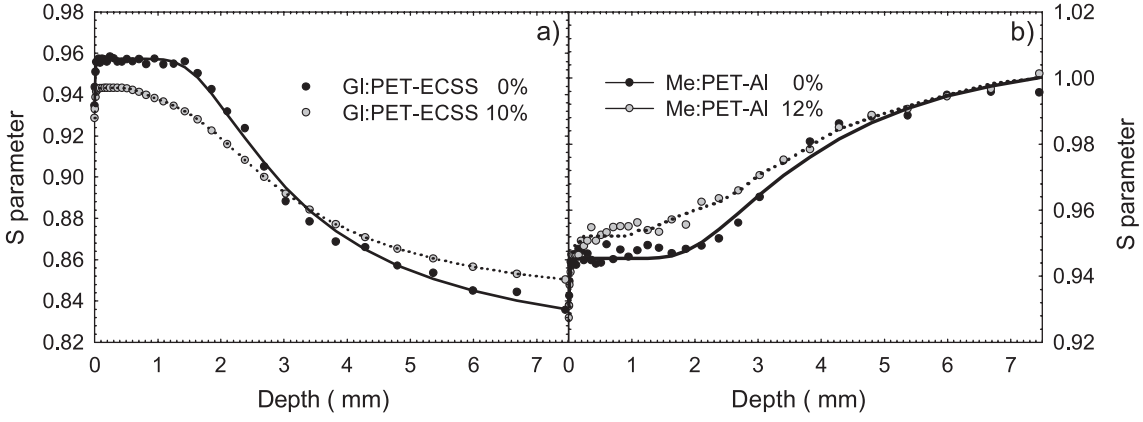

Fig. 6. Normalized S as a function of the average positron implantation depth, for sc:PET–ECCS (a), at 0% strain and 10% strain. (b) Normalized S for a sc:PET–Al, at 0% and 12% strain. Solid lines represent VEPFIT analysis results.

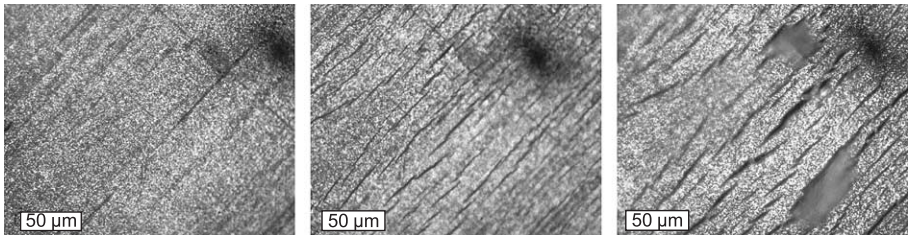

Fig. 7. Polarisation microscopic images of 4 μm sc:PET–Al laminate, at 0% (left), 5% (middle) and 8% strain (right).

(For samples that show a gradient, the average of the minimum and maximum values is plotted).

The very thin 0.3-μm PETG coated on polished IF steel showed different behavior, no cracks were observed in the coating, even at 20% strain, and a decrease of S at increasing strain was observed. This sample initially showed a higher S value when compared to the other PETG coatings (see Fig. 2). The reason for these peculiarities is not clear.

Fig. 6 shows $S(E,\varepsilon)$ as a function of depth for the Gl:PET–ECCS (a) and Me:PET–Al (b) substrates. In accordance with Eq. (4), it is found that for all depths associated with the PET coating, $S(E,\varepsilon)$ is higher in the Me:PET–Al laminate. For the Gl:PET–ECCS laminate $S(E,\varepsilon)$ is indeed lower for depths associated with the PET coating, but inside the steel substrate the values become higher indicating an increased open volume due to the deformation of the steel.

Employing Eq. (4), the fraction f_s of the crack area exposing the metal substrate, was approximated to be 7% for the Me:PET–Al laminate and 11% for the Gl:PET–ECCS laminate, which are reasonable values, considering the optical microscopic evidence (e.g. Fig. 7 for Me:PET–Al).

4. Conclusions

Positron annihilation techniques were applied to PET–metal laminates. A number of interesting results were obtained. The S parameter of PET is found to be related, roughly inversely proportional, to its crystallinity. It was established that polymer–metal interfaces may be detected with VEP-DBAR techniques if the S parameter of a polymer coating is lower than that of the metal substrate, and higher than that of the surface, and that substrates with a large diffusion length are favorable for interface detection. In the case of PET, this means that PET–Al may be an interesting system to study. It was found that the roughness of the metal substrate is of importance, rough interfaces being more difficult to observe. Changes observed in the $S(E,\varepsilon)$ parameter as a function of strain, are in agreement with a simple picture that includes a small increase in S caused by increased defect density and a large decrease or increase (depending on whether $S_s(\varepsilon)<S_{\mathrm{PET}}(\varepsilon)$ or $S_s(\varepsilon)>S_{\mathrm{PET}}(\varepsilon)$) caused by the appearance of cracks in the coating. The observed differences in the behavior of $S(E,\varepsilon)$ between laminates with amorphous and semicrystalline PET are in agreement with differences in material behavior between amorphous and semicrystalline PET.

Acknowledgement

It is with deep sorrow that we have to report the sudden death of Prof. A. van Veen during the preparation of this manuscript. The work described in this paper was supported by the Dutch Technology Foundation (STW) under grant GNS.4901.

References

[1] T.J. Pecorini, R.W. Hertzberg, Polymer 34 (1993) 5053.
[2] R. Rastogi, W.P. Vellinga, S. Rastogi, C. Schick, H.E.H. Meijer, J. Polym. Sci., Part B, Polym. Phys. 42 (2004) 2092.
[3] W.P. Vellinga, R. Rastogi, H.E.H. Meijer, in: C.S. Ozkan, L.B. Freund, R.C. Cammarata, H. Gao (Eds.), Thin Films-Stresses and Mechanical Properties IX, Boston, U.S.A., November 26–30, 2001, Materials Research Society Symposium Proceedings, vol. 695, 2002, p. 21.
[4] R. Rastogi, PhD thesis, College van Dekanen, Eindhoven University of Technology, the Netherlands (2003).
[5] A. van Veen, H. Schut, P.E. Mijnarends, in: P.G. Coleman (Ed.), Positron Beams and Their Applications, World Scientific Publishing, 2002, Chapt. 6.
[6] R.M. Mininni, R.S. Moore, J.R. Flick, S.E.B. Petrie, J. Macromol. B-8 (1–2) (1973) 343.
[7] B. Wang, Z.F. Wang, M. Zhang, W.H. Liu, S.J. Wang, Macromolecules 35 (2002) 3993.
[8] H. Cao, J.P. Yuan, R. Zhang, C.S. Sundar, Y.C. Jean, R. Suzuki, T. Ohdaira, B. Nielsen, Appl. Surf. Sci. Lett. 149 (1999) 116.
[9] M. Madani, R.R. Miron, R.D. Granata, J. Coat. Technol. 872 (1997) 45.
[10] T. Wider, K. Maier, U. Holzwarth, Phys. Rev., B 60 (1999) 179.
[11] R. Escobar Galindo, PhD thesis, College van Dekanen, Delft University of Technology, the Netherlands (2003).
[12] R. Escobar Galindo, A. van Veen, A. Alba Garcia, H. Schut, J.Th.M. De Hosson, Acta Mater. 48 (2000) 4743.
[13] A. van Veen, J. Trace Microprobe Tech. 8 (1990) 1.
[14] A. van Veen, H. Schut, J. de Vries, R.A. Hakvoort, M.R. Ijpma, in: P.J. Simpson (Ed.), Positron Beams for Solids and Surfaces, AIP, vol. 218, 1990, p. 171.
[15] A.V. Fedorov, H. Schut, A. van Veen, Mat. Sci. Forum 646 (2000) 363.
[16] G. Brauer, W. Anwand, W. Sorupa, A.G. Revesz, J. Kuriplach, Phys. Rev., B 66 (19) (2002) 195331.
[17] M. Clement, J. de Nijs, S.H. Balk, P.A. van Veen, J. Appl. Phys. 81 (1997) 1943.
[18] J. Holgado, R. Escobar Galindo, A. van Veen, H. Schut, J.Th.M. De Hosson, A. Gonzalez-Elipe, Nucl. Instrum. Methods Phys. Res., Sect. B 194 (2002) 333.